8th International Conference on Water Resources and Arid Environments (ICWRAE 8): 369-380
22-24 January 2019*, Riyadh, Saudi Arabia*

Application of Two Remote Sensing-Based Surface Energy Balance Models for Estimating Actual Evapotranspiration in the Mascara Plain, Algeria

Abderrahmane Hamimed, Laounia Nehal, Mansour Zaagane, Bachir Benarba and Mohamed Teffahi

Laboratory of Research on Biological Systems and Geomatics, University of Mascara, Algeria

Abstract: Accurate characterization of evapotranspiration (ET) and surface energy fluxes is crucial for many agro-environmental applications. Remote sensing based energy balance models are presently most suitable for estimating evapotranspiration at both temporal and spatial scales. This study presents an intercomparison of ET maps over the Mascara plain (western Algeria) obtained with two different models: METRIC (Mapping EvapoTranspiration at high Resolution using Internalized Calibration) and T_0/VI trapezoid (Surface temperature/Vegetation Index Trapezoid Model). These two models are qualified as «residual type», because they are based on a physical approach which allows the resolution of energy balance equation, where ET is estimated as the residual term. T_0/VI trapezoid is the most used model, due to its simplicity, ease of use, few data input requirements and relatively high accuracy. It allows estimating ET directly by using the Priestley-Taylor equation. Whereas METRIC model follow a physical approach, where ET is estimated as the residual term. The data set consists of four Landsat-7 ETM+ images acquired on 3 December 2001, 5 February 2002, 26 April 2002 and 15 July 2002 and some agrometeorological field measurements. In conclusion, the results show that METRIC and T_0/VI trapezoid models provide comparable outputs and suggest that both the two models are suitable approaches for ET estimation over agricultural areas where ground information is scarce or difficult to collect.

Key words: Evapotranspiration · T_0/VI trapezoid · METRIC · Energy balance · Landsat · Algeria.

INTRODUCTION

The quantification of evapotranspiration (ET) from agricultural regions is important for agriculture water management, especially in arid and semiarid regions where water deficiency is becoming a major constraint in economic development. Satellite-based energy balance models are presently most suitable for estimating ET. This latter is a major component of the terrestrial hydrological cycle, nearly two-thirds of precipitation over land is returned back to the atmosphere by ET [1]. Inaccurate estimates of ET in these regions can cause large errors in the hydrological components prediction such as runoff and recharge, and in the associated water balance and water resources availability.

Remote sensing technology can supply land surface parameters such as albedo, vegetation indexes and surface temperature, which are necessary to remote sensing-based energy balance models for scaling up ET and surface energy fluxes to larger spatial and longer temporal scales. It is recognized as the only way to estimate ET at several temporal and spatial scales [2]. To this end, major effort has been devoted over the past to improve remote sensing-based methods that provide spatially distributed surface fluxes maps using airborne and satellite data [3]. Basically, these methods can be classified into three main categories: 1) Those using simple empirical relationships relating daily ET to an instantaneous surface temperature measurement [4]; 2) Those using deterministic relationships based on more complex models such as Soil-Vegetation-Atmosphere Transfer models (SVAT) [5]; 3) Those basing on the estimation of ET as the residual term of the energy balance equation. They can be divided into two categories:

1) Single-source models, such as SEBAL (Surface Energy Balance Algorithm for Land) [6], METRIC (Mapping Evapotranspiration with Internalized

Corresponding Author: Hamimed Abderrahmane, Laboratory of Research on Biological Systems and Geomatics, University of Mascara, Algeria. Phone/Fax: +213 45 72 28 44, E-mail: hamimed@univ-mascara.dz.

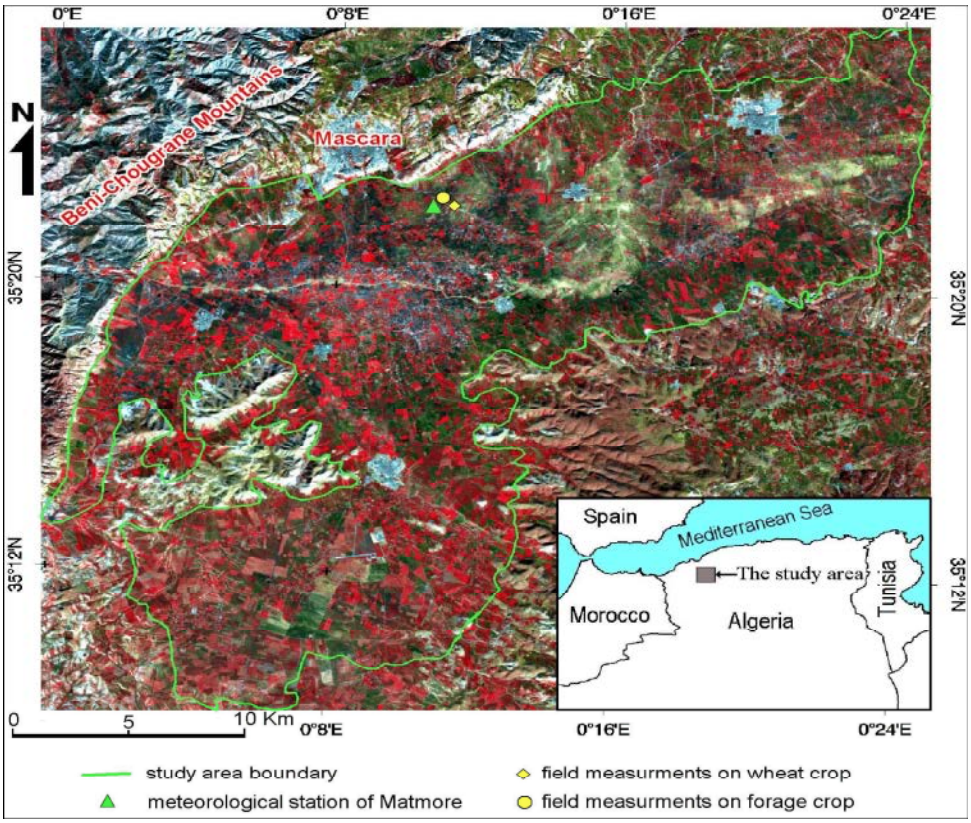

Fig. 1: Location and false color composite 4,3,2 of Landsat ETM+ imagery acquired on February 5 (DOY 36), 2002 of the study site at Mascara plain, Algeria.

Calibration) [7], S-SEBI (Simplified Surface Energy Balance Index) [8], SEBS (Surface Energy Balance System) [9] and T_0/VI trapezoid model (Surface temperature/Vegetation Index Trapezoid Model) [10], that do not distinguish between soil evaporation and transpiration. Their simplicity has made the single-source models widely used; 2) dual-source models, such as TSEB (Two Source Energy Balance) [11] and SPARSE (Soil Plant Atmosphere and Remote Sensing Evapotranspiration) [12] that discriminates the soil and vegetation component.

This study evaluates the performance of T_0/VI trapezoid and METRIC models for ET estimation. T_0/VI trapezoid allows estimating ET directly by using the Priestley-Taylor equation. It requires few input data, since it is based on a purely graphical method which allows deducing the extreme values of surface temperature from the scatterplots between vegetation index (NDVI) and surface temperature, and then the Priestley-Taylor parameter is calculated [13]. However METRIC followed an energy balance approach, where the latent heat flux (corresponding to the energetic equivalent of ET flux) is estimated as the residual term when net radiation, sensible and soil heat fluxes are known. The METRIC approach is the suitable approach for ET estimation over agricultural areas where ground information is scarce or difficult to collect [14]. Moreover, METRIC has the particularity of using the hourly reference ET in the calculation of evaporative fraction, which makes it the most suitable model for conditions with strong local advection which characterize the semiarid regions in Algeria [14].

The emphasis of this study is to use METRIC and T_0/VI trapezoid models for estimating the actual ET over a semi-arid region in Algeria, where ground data are scarce or difficult to collect. Than the estimates of these models are compared with ground observations on wheat and forage crops using the Bowen Ratio Energy Balance (BREB) method.

Study Area and Data: This study area correspond to the Mascara plain which is a semi-arid agrosystem in the north-west of Algeria, three kilometers away southward from the town of Mascara, between longitudes 0° 0’ 3" E and 0° 24' 42" E and latitudes 35° 7' 54"N and 35° 27' 34" N. It covers an area of 576 km^2 (Fig. 1).

Table 1: Landsat 7-ETM+ imagery used in the study.

(Path/Row)	Acquisition Date	Acquisition moment (GMT)	Day of the year (DOY)	Solar elevation (degree)
197/36	December 3rd, 2001	10h21'	337	29.42
197/36	February 5th, 2002	10h21'	36	32.8
197/36	April 26th, 2002	10h21'	116	60.1
197/36	July 15th, 2002	10h21'	196	64.4

Table 2: Meteorological conditions during the image acquisition of Landsat ETM+ on the selected days

Parameter	Unit	03/12/2001 (DOY 337)	05/02/2002 (DOY 36)	26/04/2002 (DOY 116)	15/07/2002 (DOY 196)
Air Temperature	°C	10.3	12.7	24	25
Relative humidity	%	82.6	68	28	39
Atmospheric Pressure	Mbar	968.7	975	965	961.4
Incoming shortwave radiation	W/m^2	456.24	566	888	906
Atmospheric radiation	W/m^2	294.4	294.4	321.1	361.6
Atmospheric transmittance	-	0.694	0.716	0.777	0.769
Wind speed	m/s	0.4	2	0.5	1.2
Daily relative sunshine duration	-	9.4	9.4	12.9	13.6
Potential evapotranspiration	mm	2	2.9	7.2	9.7

The selected area belongs to the Mascara plain which is a flat expanse of a surface of about 650 km^2 and an average altitude of 470 m, overhung by reliefs of elevated border up to 1100 m in the South. The lands outcropping are from sedimentary formation with variable texture, consisting mainly of recent and ancient alluvium. Soils are mostly of calcimagnesic type, but sometimes one meets isohumic soils and poorly evolved soils. The northern limit of the plain is distant from the Mediterranean Sea of about 50 km and its southern boundary is located at a hundred kilometers of the Saharan Atlas. Therefore, it is found submitted to Mediterranean and Saharan influences. The latter are clearly predominant due to the screen formed by the Beni-Chougrane Mountains in the North [15]. The study area is characterized by a semi-arid climate and recurrent drought. Two main periods characterize this area, a rainy and dark period during the months of November to April and another dry and hot period during the months of May to September. Winter (from December to February) is usually cold enough. The absolute minimum of the air temperature descends to -4°C. Summer (from June to August) is usually hot and dry. The absolute maximum of the air temperature is equal to +42 °C. Thermal maxima are accentuated by the sirocco, a hot drying wind from the South. Rainfall is concentrated during the cold period. The annual rainfall for the period 1922-1989 oscillates between 300 and 600 mm, with an average of 420 mm [15]. March, April, November and December are the rainiest months of the year, while June, July and August are the hottest months.

Remote sensing data used in this study consists of four Landsat-7 ETM+ (Enhanced Thematic Mapper Plus) imagery acquired during 2001 and 2002 (Table 1). These data are supplemented by ground measurements which were performed on two points located in the experimental site of the university of Mascara. The first point was located on wheat crop and the second on forage crop (Fig. 1). These measurements were intended for the daily monitoring of energy fluxes at the soil-plant-atmosphere interface [16]. They correspond to the radiometric surface temperature, the reflected radiation and the three components of surface energy balance, i.e. soil heat flux (G), sensible heat flux (H) and latent heat flux (λE). Incoming shortwave (solar) and thermal radiations were measured on the meteorological station of Matmore (ONM), located in the study area (Fig. 1) using a pyranometer and a pyrgeometer, respectively. The meteorological station also provided measurements on the reference variables which are air temperature, air humidity, wind speed, air pressure, sunshine duration and daily potential ET (Table 2). On the experimental device, installed on the plots of wheat and forage, the albedo was given by the ratio of the reflected radiation and the incoming shortwave radiation. The net radiation (Rn) is determined from the radiative balance equation, depending on the albedo, the incoming shortwave and thermal radiations and the surface emission which is deduced from the radiometric surface temperature (measured by a IRTS-P model Apogee infrared radiometer). The soil heat flux (G) is measured using Hukseflux conductive flux plates installed at 5 cm depth in the soil. Sensible and latent heat fluxes were computed from measurements at two levels (0.5 and 2.5 m above the surface) of air temperature and relative humidity using the BREB technique.

Models Description

Mapping EvapoTranspiration with Internalized Calibration (METRIC) Model: For the determination of ET, METRIC estimates the latent heat flux (λE) as the residual term of the energy balance equation. This latter describes the energy exchange between the land surface and the atmosphere:

$$\lambda E = Rn - G - H \quad (1)$$

where Rn is the net radiation at the surface (W/m^2), H is the sensible heat flux (W/m^2), G is the soil heat flux (W/m^2) and λE is the latent heat flux (energy consumed by ET, W/m^2). Net radiation (Rn) estimation is quite similar for both models; it is calculated according to:

$$Rn = (1 - r_0) \cdot Rg + L^{\downarrow} - L^{\uparrow} \quad (2)$$

where Rg is the incoming shortwave radiation, partly reflected depending on the albedo r_0, $L^{\downarrow}$ and $L^{\uparrow}$ are the incoming and the emitted outgoing longwave radiations (W/m^2), respectively.

Mapping the net radiation (Rn) requires evaluation of the incoming shortwave radiation (Rg), the outgoing longwave radiations ($L^{\uparrow}$) (obtained by the expression of Stephan-Boltzmann) and the incoming longwave radiation ($L^{\downarrow}$), using air temperature and atmosphere emissivity. This latter is calculated depending on atmospheric transmittance (τ) following the expression [6]:

$$\varepsilon_a = 1.08 \times (-\ln \tau)^{0.265} \quad (3)$$

The soil heat flux (G) is estimated using the following relation suggested by [6]:

$$G = T_0 (0.0032 + 0.0062\, r_0) \times (1 - 0.978\, (NDVI)^4) \times Rn \quad (4)$$

The sensible heat flux (H) is expressed as a function of the near-surface air temperature difference (T_{aero}-T_a) as follows:

$$H = \frac{\rho . Cp}{r_{ah}} (T_{aero} - T_a) \quad (5)$$

where ρ is air density (kg/m^3), Cp is air specific heat at constant pressure (J/kg/K), T_{aero} is the aerodynamic temperature (K), T_a is the air temperature (K) and r_{ah} is the aerodynamic resistance to heat transfer. In satellite remote sensing applications, the radiometric surface temperature (T_0) retrieval is often used instead of the aerodynamic temperature (T_{aero}) in Eq. (5) [17]:

In METRIC, the sensible heat flux (H) is estimated using the following expression:

$$H = \frac{\rho \cdot Cp}{r_{ah}} dT \quad (6)$$

where dT is the near-surface temperature difference between two near surface heights z_1 = 0.1 m and z_2 = 2 m above the canopy layer, and r_{ah} is the aerodynamic resistance to heat transport between these levels (s/m). dT is used in Eq. (6) because of the difficulty in estimating surface temperature T_0 accurately from satellite due to uncertainty in atmospheric attenuation or contamination and radiometric calibration of the sensor [7]. In addition, T_0, as measured by satellite (i.e., radiometric or kinetic temperature) can deviate from the "aerodynamic" temperature that drives the heat transfer process by several degrees [18], following [6].

In METRIC, r_{ah} is calculated between z_1 and z_2 using a wind speed extrapolated from some blending height above the surface (~200 m) and an iterative procedure for correcting atmospheric stabilities to heat and momentum transfer, based on the Monin-Obukhov's similarity theory.

In this model, the difference dT between the two near surface heights 0.1 and 2 m is approximated by a simple linear function:

$$dT = a \cdot T_0 + b \quad (7)$$

The coefficients a and b in Eq. (7) are empirically determined using the properties of pixels in extreme water conditions (hot/cold and dry/wet). These pixels are identified on the image by analyzing the vegetation index and the surface temperature relationship according to the triangle method [14]. The dry pixels are indicated at bare soils (NDVI values close to zero) having high surface temperature. However, the wet pixels are indicated at fully vegetation (NDVI >0.7) having low surface temperature. The thresholds of low and high temperatures are defined as the equilibrium surface temperatures resulting from the energy balance for well-watered dense vegetation and dry bare soil, respectively [19].

With the identification of wet and dry pixels, we can determine H_{wet} and H_{dry} from the energy balance equation as follows:

$$H_{wet} = (Rn - G)_{wet} - \lambda E_{wet} \quad (8)$$

$$H_{dry} = (Rn - G)_{dry} - \lambda E_{dry} \quad (9)$$

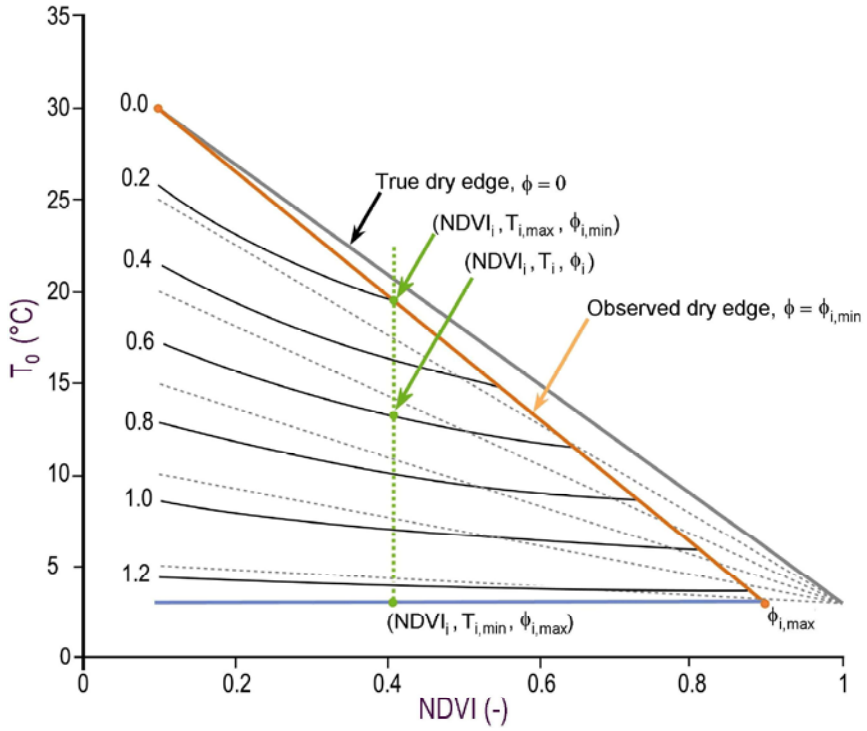

Fig. 2: Illustration of the conceptual dT_S-NDVI plot. The true dry edge (grey) representing zero ET ($\phi_{i,min}$ =0), the observed dry edge (red) representing limiting ET ($\phi_{i,min}$) and the wet edge (blue) representing potential ET (ϕ_{max}). Dashed grey and solid black lines are iso-lines of equal moisture availability and ϕ respectively. (After [10]).

A dry pixel is characterized by a zero latent heat flux (λE_{dry} = 0), which means, the overall available energy $(Rn- G)_{dry}$ is partitioned into sensible heat flux. For a wet pixel, the latent heat flux (λE_{wet}) in METRIC is assumed to be equal to the hourly reference evapotranspiration ETr, estimated for a hypothetical reference crop, alfalfa, by using Penman-Monteith equation [20] multiplied by an empirical coefficient of 1.05. The choice of this coefficient is primarily dictated by the assumption that a wet pixel (fully covered by vegetation) usually has an ET value of 5% larger than ETr [7].

With the calculation of H_{wet} and H_{dry}, Eq. (6) was inverted to compute dT_{wet} and dT_{dry}. The use of Eq. (6) enables us to compute the sensible heat flux in pixel basis and solving the energy balance equation. This step leads mapping the latent heat flux. This should help in the interpretation of a surface behaviour with respect to water stress [6].

T_0/VI trapezoid Model: The relation between surface temperature (T_0, or surface-air temperature difference dT_s) and vegetation index (the normalized difference vegetation index (NDVI)) has been widely used to obtain information about the energy fluxes or soil moisture of the land surface [10, 21, 22]. Scatterplots between remotely sensed T_0 and NDVI often results in a trapezoidal/triangular shape (Fig. 2). The prerequisite for estimating evaporative fraction (EF) and ET from the T_0/VI trapezoid is to determine accurately the lower edge of this space (wet edge) which is characterized by saturated surface soil water content with maximum ET and the upper edge (dry edge) of the scatter plot representing lower limit of surface soil moisture content with limited ET and higher limit of surface temperature for a given NDVI [23]. The T_0/VI method should ideally be applied over smaller regions and those with little topographic variation.

The four points of the trapezoid corresponds to extreme conditions of surface in terms of surface temperature and NDVI, which allow deducing the extreme values of surface temperature and NDVI [22].

The Priestley-Taylor formulation [24] with fully remotely sensed data proposed by [22] and further improved and validated by [10] representatively based on the interpretations of the T_0/VI trapezoid model, has been employed to estimate ET using the following equation:

$$\lambda E = \phi \left[(Rn - G) \frac{\Delta}{\Delta + \gamma} \right] \quad (10)$$

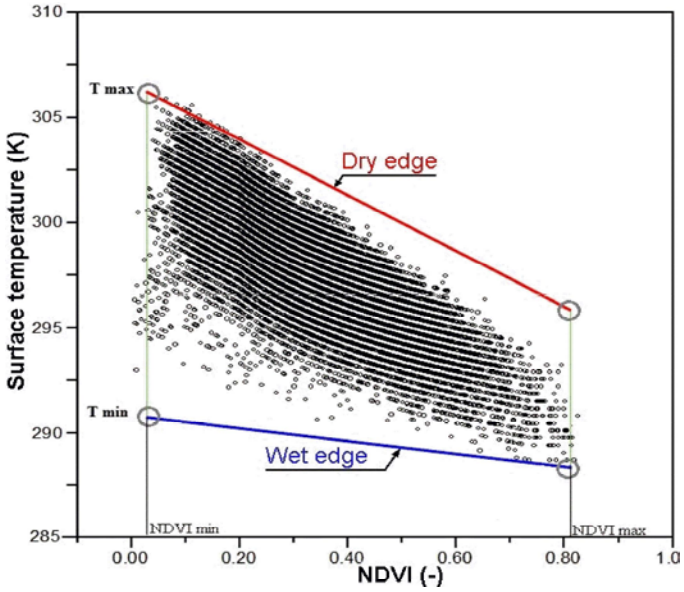

Fig. 3: Illustration of the trapezoid method used for identifying wet and dry pixels (DOY 36).

where γ is the psychrometric constant (≈0.66 mbar.K^{-1}) and Δ is the slope of the saturation vapor curve at air temperatures (T_a), calculated with:

$$\Delta = \frac{2503.058}{(T_a + 237.3)^2} \exp\left(\frac{17.27\, T_a}{T_a + 237.3}\right) \quad (11)$$

Eq. (10) is a modified version of the Priestley-Taylor equation in the case of unsaturated surfaces by the introduction of the parameter ϕ which represents the so-called Priestley-Taylor parameter, and which accounts for aerodynamic and canopy resistances, and is slightly different from the original Priestley-Taylor's parameter α (~1.26). This parameter depends on surface moisture conditions [25]. It is defined globally to range from ϕ_{min}= 0, for a dry bare soil, to ϕ_{max}= (Δ+γ)/Δ, for a saturated or well vegetated surface.

As illustrated in Fig. 3, ϕ_{min} is assigned to a pixel with minimum NDVI and maximum temperature; ϕ_{max} is assigned to pixels with maximum NDVI.

ϕ can be expressed as a function of the evaporative fraction (EF) as follows:

$$\phi = EF \cdot \frac{\Delta + \gamma}{\Delta} \quad (12)$$

where EF is defined as the ratio of ET or latent heat flux (λE) to available energy (Rn-G):

$$EF = \frac{\lambda E}{H + \lambda E} = \frac{\lambda E}{Rn - G} = \phi \frac{\Delta}{\Delta + \gamma} \quad (13)$$

The parameter ϕ is estimated following the approach proposed by [22] using three steps [10]: In the first step, surface moisture condition is estimated by interpolating the surface temperature between the wet and dry edges. The dry and wet edges are experimentally or theoretically identified by determining the surface temperature in the trapezoid corners (Fig. 3) using surface energy balance equation and boundary conditions represented by the surface resistances values for each moisture condition for soil and vegetation. In this study, we set a surface resistance of 10 s/m for wet vegetation cover, 400 s/m for dry vegetation cover, 0 for wet bare soil and 8 for dry bare soil [26].

In the second step, we estimate $\phi_{i,min}$ which represents the minimum value of ϕ for a given fraction cover (f_c) value, as:

$$\phi_{i,\min} = \phi_{\max} \cdot f_c \quad (14)$$

where $\phi_{i,min}$ is the value of the Priestley-Taylor parameter at the dry edge for a given value of NDVI$_i$, ϕ_{max} is the value of ϕ at the wet edge (ϕ_{max} =(Δ+γ)/Δ).
The fraction cover (f_c) is expressed as [10]:

$$f_c = \left(\frac{NDVI - NDVI_{\min}}{NDVI_{\max} - NDVI_{\min}}\right)^2 \quad (15)$$

where NDVI$_{min}$ and NDVI$_{max}$ are the minimum and maximum observed vegetation index values, corresponding respectively to bare soil and fully vegetated surfaces, defining the extremes of the trapezoid.

The third step is to interpolate ϕ between $\phi_{i,min}$ and $\phi_{i,max}$ within each NDVI class between the lowest temperature ($T_{s,i,min}$) at wet edge and highest temperature ($T_{s,i,max}$) at dry edge. The linear interpolation of ϕ_i with temperature leads to normalization of surface temperature and is given as:

$$\phi_i = \frac{T_{0,i,\max} - T_{0,i}}{T_{0,i,\max} - T_{0,i,\min}}\left(\phi_{\max} - \phi_{i,\min}\right) + \phi_{i,\min} \quad (16)$$

where $T_{s,i,min}$ is the lowest surface temperature at the wet edge for a given NDVI and $T_{s,i,max}$ is the highest temperature at the dry edge for a given NDVI.

RESULTS AND DISCUSSION

Both METRIC and T_0/VI trapezoid models are developed in C++ code. In the studies of ET estimation through the energy balance equation, the sensible heat flux evaluation is the most delicate for residual models such as METRIC. In his approach, [27] used an empirical method to reduce errors due to this flux. However, the approach used in our study is based on the Monin-Oubukhov's similarity theory in the atmospheric boundary layer. In fact, the surface boundary layer modeling allows mapping the sensible heat flux which is obtained by estimating two key parameters of the energy balance regulation, depending on the surface type and its thermodynamic properties which are the aerodynamic resistance to heat transfer (r_{ah}) and the surface-air temperatures difference.

In the sensible heat flux (H) estimation, wet pixels are identified on dense vegetation cover (NDVI> 0.7), with an average temperature values of 286.3 K, 287.1 K, 301.2 K and 304.8 K for the DOY 337, 36, 116, 196, respectively (Table 3). We note also on Table 3 that for dry pixels (bare soil and urban) the aerodynamic resistance to heat transfer (r_{ah}) is low (21.88 s/m, 18.55 s/m, 14.91 s/m and 17.38 s/m for the DOY 337, 36, 116, 196, respectively), causing the release of sensible heat to the atmosphere. This is justified by high differences between surface and air temperatures. However, for wet pixels (freshly irrigated plots) r_{ah} values are high (35.42 s/m, 37.96 s/m, 120.61 s/m and 56.48 s/m for the DOY 337, 36, 116, 196, respectively) because the net available energy (Rn-G) is mainly consumed by ET. This differentiation of the sensible heat flux for dry and wet pixels is caused by the surface water status and its influence on the energy partition between the latent and sensible heat. Specifically, wet surfaces are individualized by low H values while high H values are assigned to dry areas (Table 3).

The latent heat flux (λE) is the energy consumed by ET. It is generally high for dense canopy and low for dry bare soils having high surface temperatures, low net radiations and high sensible heat fluxes. Table 4 summarizes the results of energy fluxes and moisture indicators obtained from the two models (METRIC and T_0/VI trapezoid) for different land use categories. It shows that high values of latent heat flux are observed on the irrigated areas with dense vegetation, while low values are on the bare soils, corresponding to high values of albedo. This allows emphasizing that the spatial distribution of METRIC and T_0/NDVI trapezoid-derived ET is correlated to the water regimes of the different land use units.

Table 3: Instantaneous average values of parameters and surface energy fluxes above dry and wet pixels in the study area

			Image 03/12/2001 (DOY 337)		Image 05/02/2002 (DOY 36)		Image 26/04/2002 (DOY 116)		Image 15/07/2002 (DOY 196)	
Parameter	Notation	Unit	Dry pixels	Wet Pixels	Dry pixels	Wet Pixels	Dry pixels	Wet Pixels	Dry pixels	Wet Pixels
NDVI	NDVI	-	0.11	0.8	0.08	0.81	0.15	0.86	0.14	0.76
Albedo	r_0	-	0.16	0.21	0.14	0.23	0.19	0.22	0.21	0.22
Emissivity	ϵ_0	-	0.91	0.99	0.91	0.99	0.92	0.99	0.92	0.99
Surface Temperature	T_0	K	305.11	286.4	305.22	287.1	328.79	301.2	331.5	304.8
Net radiation	Rn	$W.m^{-2}$	191.22	259.51	297.17	330.79	408.19	554.5	405	558.61
Soil heat flux	G	$W.m^{-2}$	25.53	9.11	39.24	13.10	99.68	31.83	106.86	54.12
Friction velocity	u*	$m.s^{-1}$	0.19	0.2	0.19	0.2	0.088	0.061	0.14	0.13
Monin-Oubukhov length	L	m	-3.99	-80.66	-3.03	-204.66	-0.2	-12.51	-1.03	-35.43
Aerodynamic resistance to heat transport	r_{ah}	$s.m^{-1}$	21.88	35.42	18.55	37.96	14.91	120.61	17.38	56.48
Sensible heat flux	H	$W.m^{-2}$	172.25	0	254.81	0	307.9	0	296.66	0
Latent heat flux (METRIC)	λE	$W.m^{-2}$	0	245.15	0	316.62	0	521.89	0	502.13
Evaporative fraction (METRIC)	EF	-	0	1	0	1	0	1	0	1
Latent heat flux (TIM)	λE	$W.m^{-2}$	0	250.51	0	316.62	0	522.67	0	504.04
Evaporative fraction (TIM)	EF	-	0	1	0	1	0	1	0	1
Near-surface and air temperature différence	dT	° C	21.64	0	19.36	0	31.62	0	32.88	0

Table 4: Variation of surface energy fluxes and moisture indicators with land use in the Mascara plain.

				METRIC			T_0/NDVI trapezoid		
Satellite image date	Type of land use	Rn	G	H	λE	EF	ϕ	λE	EF
03/12/2001 (DOY 337)	Bare soil	223.72	18.43	73.25	132.04	0.64	1.11	127.27	0.62
	Sparse vegetation	253.67	19.51	46.67	187.49	0.80	1.38	180.30	0.77
	Moderate Vegetation	271.65	16.27	24.31	231.07	0.90	1.63	232.39	0.91
	Dense Vegetation	270.36	13.12	12.38	244.86	0.95	1.70	244.37	0.95
	Very dense Vegetation	261.12	10.21	8.67	242.24	0.97	1.75	245.89	0.98
05/02/2002 (DOY 36)	Bare soil	302.75	34.87	142.19	122.04	0.46	0.64	101.79	0.38
	Sparse vegetation	309.88	32.5	108.85	165.6	0.60	0.93	152.55	0.55
	Moderate Vegetation	321.13	28.63	74.78	215.45	0.74	1.20	207.67	0.71
	Dense Vegetation	326.34	23.04	43.31	258.29	0.85	1.40	251.73	0.83
	Very dense Vegetation	326.05	18.11	25.07	281.55	0.91	1.58	289.46	0.94
26/04/2002 (DOY 116)	Bare soil	421.07	94.31	189.4	137.36	0.41	0.51	120.90	0.37
	Sparse vegetation	459.13	92.15	131.64	235.33	0.63	0.71	190.82	0.52
	Moderate Vegetation	514.99	81.46	52.92	380.6	0.87	1.11	351.15	0.81
	Dense Vegetation	536.84	67.34	26.07	443.42	0.94	1.18	403.77	0.86
	Very dense Vegetation	539.48	53.15	15.5	470.82	0.96	1.30	462.01	0.95
15/07/2002 (DOY 196)	Bare soil	415.29	103.26	202.43	109.58	0.34	0.51	118.57	0.38
	Sparse vegetation	464.58	101.46	137.88	225.23	0.61	0.80	214.24	0.59
	Moderate Vegetation	436.9	90.6	62.14	374.75	0.85	1.13	290.89	0.84
	Dense Vegetation	542.07	75.29	32.32	434.44	0.92	1.27	438.77	0.94
	Very dense Vegetation	548.2	60.88	14.58	472.74	0.96	1.31	472.70	0.97

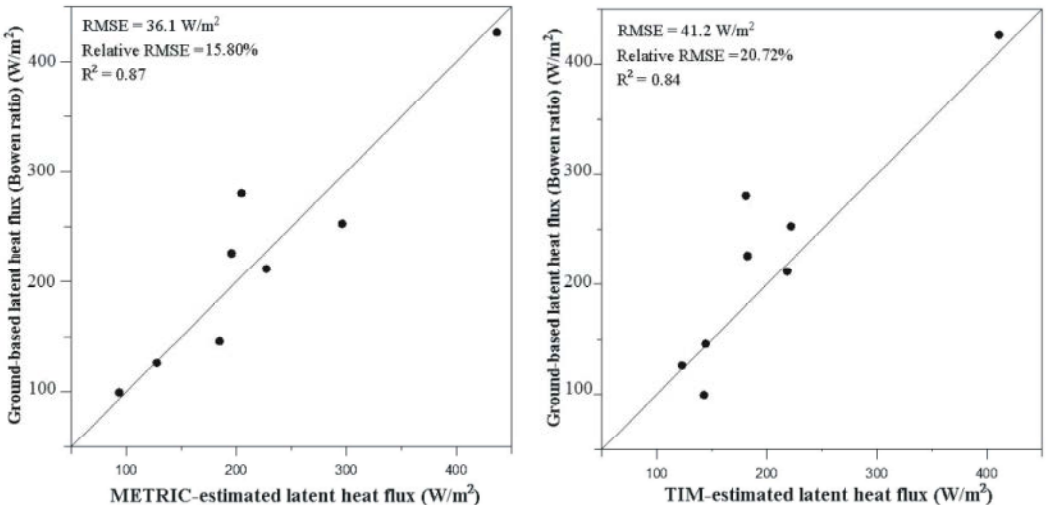

Fig. 4: Comparison of ground-based and satellite-derived estimates of latent heat fluxes: METRIC model (left) and T_0/VI trapezoid model (right).

A method commonly used to validate the obtained results is to compare latent heat flux values obtained by METRIC and T_0/VI trapezoid models from the image with those estimated on the ground using the BREB technique. [28] indicated that this technique have ~20% uncertainty, hence, when discrepancies between model predicted and ground observed heat fluxes are less than ~20%, the performance of model is deemed acceptable. The result of comparison between remote sensing-estimated and ground-measured latent heat flux is shown in Fig. 4 which indicates a slight discrepancy, with a root mean square error (RMSE) of 36.1 $W.m^{-2}$ for METRIC and 41.2 $W.m^{-2}$ for T_0/VI trapezoid, which correspond to 15.80% and 20.72% in relative values and a determination coefficients (R^2) of 0.87 and 0.84 respectively. This result is closely similar to that obtained on the Low-Middle Sγo Francisco River basin in Brazil (RMSE = 33.8 W/m^2) by [29]. This shows significant correlations to justify that both approaches (METRIC and T_0/VI trapezoid) applied to the Mascara site are promising for remotely sensed ET monitoring.

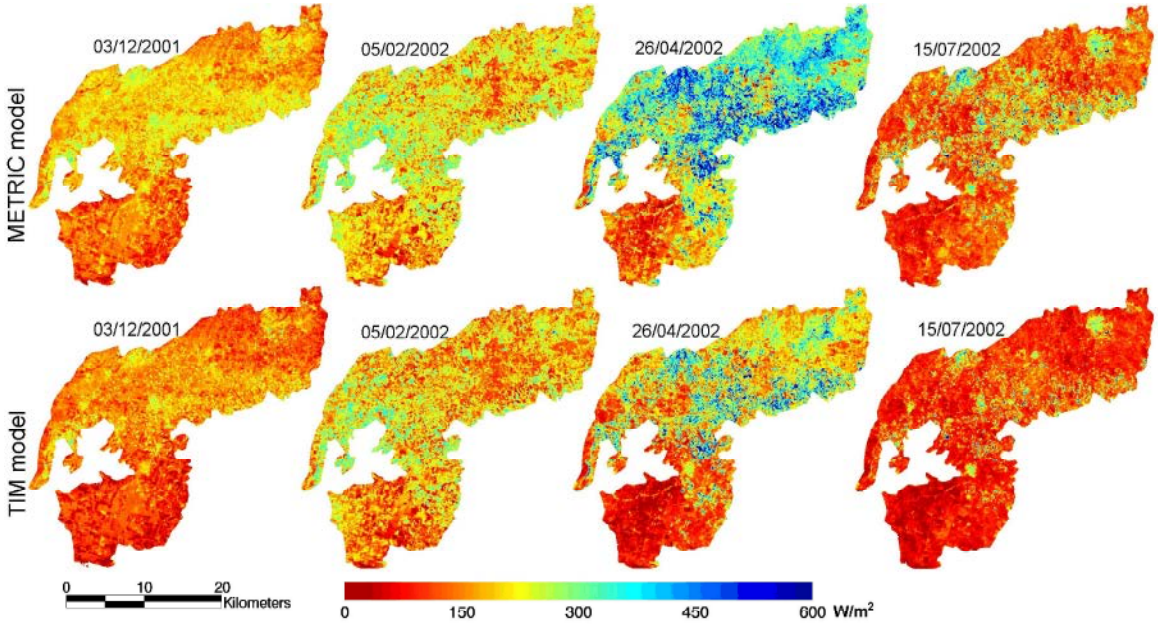

Fig. 5: Spatial distributions of latent heat flux estimated with METRIC and TIM on December 3rd, 2001, February 5th, 2002, April 26th, 2002 and July 15th, 2002.

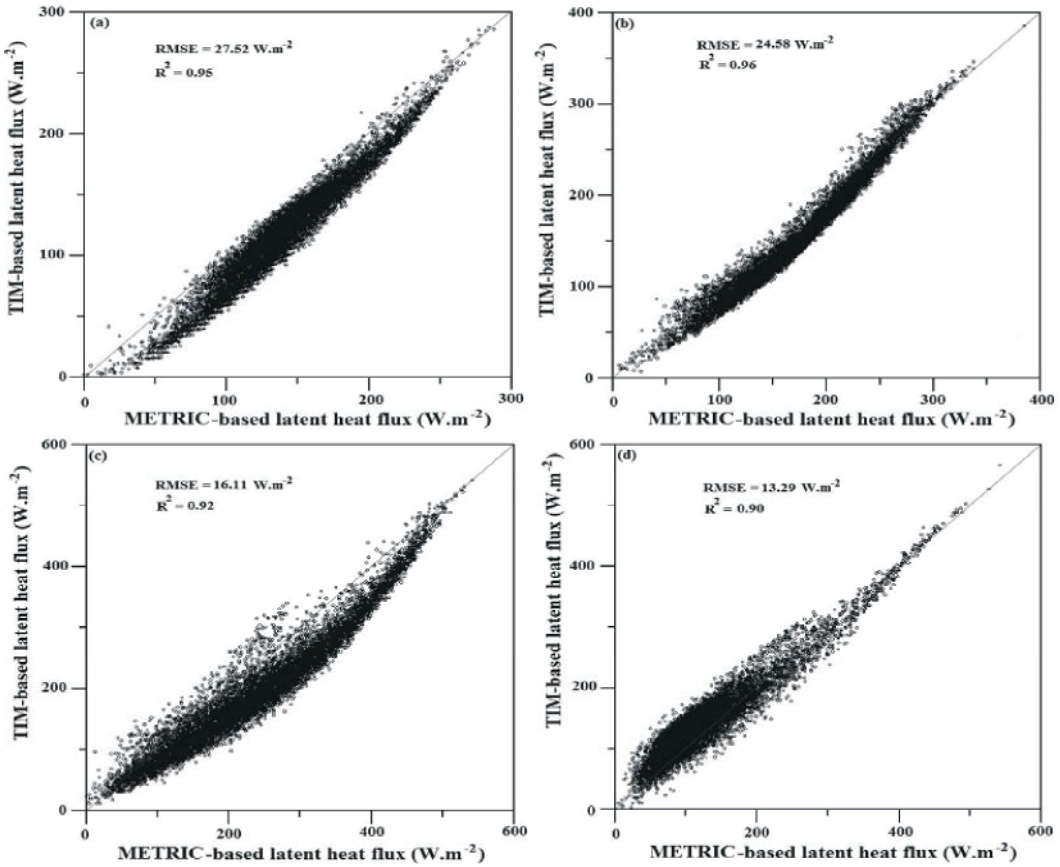

Fig. 6: Comparison of the latent heat flux estimates with METRIC and TIM on December 3rd, 2001 (a), February 5th, 2002(b), April 26th, 2002 (c) and July 15th, 2002 (d) over the Mascara plain.

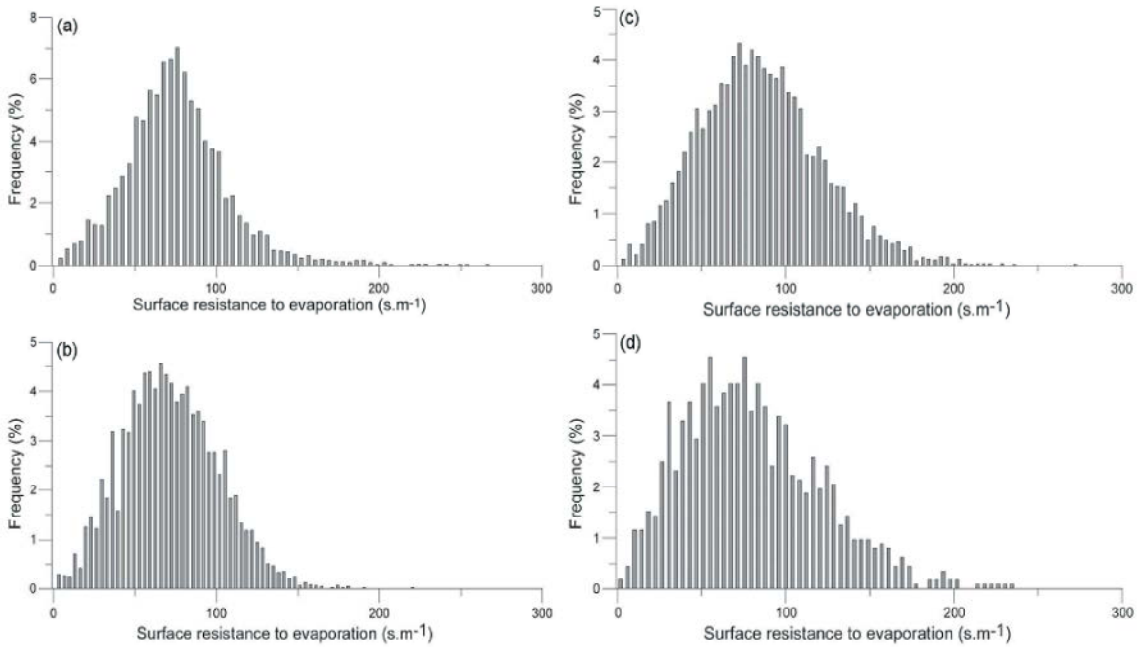

Fig. 7: Frequency distributions of the surface resistance to evaporation estimated with METRIC on December 3rd, 2001 (a), February 5th, 2002(b), April 26th, 2002 (c) and July 15th, 2002 (d) for pixels with NDVI values more than 0.6.

Figure 5 shows the spatial distributions of latent heat fluxes (λE) derived from the two models. It illustrates that the METRIC predicted a slightly higher λE than the T_0/VI trapezoid. These spatial patterns are likely due to different approaches used to estimate H and λE by the two models. The METRIC calculates H using a single-source temperature gradient technique for heat transport, accounting for stability effects based on the Monin–Obukhov theory, and λE is computed as a residual of the energy balance equation, while the T_0/VI trapezoid calculates λE directly from equation (16), but H is calculated as a residual of the energy balance equation. Based on the identified spatial patterns for H and λE, the METRIC computational scheme seems to be more physically comprehensive considering the stability for the aerodynamic resistance of heat transport [30].

The comparison of the latent heat flux estimates with METRIC and T_0/VI trapezoid is shown in Fig. 6. In general, a strong correlations of 0.95, 0.96, 0.92 and 0.90 is shown for the DOY 337, 36, 116 and 196 respectively, with an RMSE of 27.52 W.m^{-2}, 24.58 W. m^{-2}, 16.11 W. m^{-2} and 13.29 W. m^{-2} respectively (Fig. 6). The result of this comparison leads to the conclusion that the two models provide comparable outputs and suggests that both models can be considered as operational approaches for monitoring ET over agricultural areas having limited amount of ground information.

The analysis of the frequency distribution of surface resistance to evaporation, illustrated in figure 7, is another way to validate our results. [31] showed that for most crops covering fully soil, this resistance vary between 10 and 300 sm^{-1} with generally peaking in the class of 30 to 80 s m^{-1}. There is a general consensus that the surface resistance for crops which cover the soil entirely lies in approximately the same range [32]. The results shown in Fig. 7 are approximately consistent with this indication.

CONCLUSION

Different models have been developed to estimate ET from remote sensing data. In this paper, METRIC and T_0/VI trapezoid models were applied using Landsat ETM+ data over the Mascara plain (western Algeria), a semiarid region with heterogeneous surface conditions, to estimate actual ET. The models outputs were compared with field observations using the Bowen ratio energy balance method, to identify the most appropriate model.

A significant discrepancy between remote sensing and ground estimates of latent heat flux is shown, with an RMSE values of 36.1W/m^2 and 41.2 W/m^2 for METRIC and TIM respectively, i.e. 15.80% and 20.72% in relative terms and a determination coefficients (R^2) of 0.87 and 0.84 respectively, that is ascribed to errors committed in estimating the net radiation, soil heat flux and the sensible

heat flux, which correspond to the RMSE between estimates and measurements of 8.71 W/m^2 (2.7%), 13.2 W/m^2 (27.43%), 36,1 W/m² (15.80%) with METRIC model 41.2 W/m² (20.72%) with T_0/VI trapezoid, respectively. These differences can be explained by the inaccuracies on the intermediate variables such as surface emissivity, soil heat flux, roughness length and air temperature.

The results presented above confirm the possibilities offered by the Landsat ETM + satellite data to solve the energy balance equation, and to estimate ET. Despite these inaccuracies, the results show that the two models METRIC and T_0/VI trapezoid provide comparable outputs and suggest that both models are suitable approaches to estimate actual ET from agricultural areas where ground information is scarce or difficult to collect.

REFERENCES

1. Brutsaert, W., 1982. Evaporation into the atmosphere. Reidel D Publishing Company, Boston, Massachusets, pp: 299.
2. Gomez, M., A. Olioso, J.A. Sobrino and F Jacob, 2005. Retrieval of Evapotranspiration Over the Alpilles/ReSeDA Experimental Site Using Airborne POLDER Sensor and a Thermal Camera. Remote Sens Environ., 96: 399-408.
3. Khaldi, A., A. Hamimed, K. Mederbal and A. Seddini, 2011. Obtaining evapotranspiration and surface energy fluxes with remotely sensed data to improve agricultural water management. African Journal of Food. Agriculture. Nutrition and Development 11(1).
4. Trezza, R., 2006. Evapotranspiration from a Remote Sensing Model for Water Management in an irrigation system in Venezuela. Interciencia, 31(6): 417-423.
5. Olioso, A., Y. Inoue, S. Ortega-Farias, J. Demarty, J.P. Wigneron, I. Braud, F. Jacob, P. Lecharpentier, C. Ottlé, J.C. Calvet and N. Brisson, 2005. Future directions for advanced evapotranspiration modeling: assimilation of remote sensing data into crop simulation models and SVAT models. Irrigation and Drainage Systems, 19: 377-412.
6. Bastiaanssen, W.G.M., M. Menenti, R.A. Feddes and A.A.M. Holtslag, 1998. A remote sensing surface energy balance algorithm for land (SEBAL): 1. Formulation. J. Hydrol., 198-212: 212-213.
7. Allen, R.G., M. Tasumi and R. Trezza, 2007. Satellite-based energy balance for mapping evapotranspiration with internalized calibration (METRIC) - model. ASCE J. Irrig. Drain. Eng., 133: 380-394.
8. Roerink, G.J., Z. Su and M. Menenti, 2000. S-SEBI: A simple remote sensing algorithm to estimate the surface energy balance. Physics and Chemistry of the Earth, Part B: Hydrology, Oceans and Atmosphere, 25(2): 147-157.
9. Su, Z., 2002. The Surface Energy Balance System (SEBS) for estimation of turbulent heat fluxes atscales ranging from a point to a continent. Hydrol Earth Sys. Sci., 6(1): 85-99.
10. Stisen, S., I. Sandholt, A. Norgaard, R. Fensholt and K.H. Jensen, 2008. Combining the triangle method with thermal inertia to estimate regional evapotranspiration—applied to MSG-SEVIRI data in the Senegal River basin. Remote Sensing of Environment, 112(3): 1242-1255.
11. Norman, J.M., W.P. Kustas and KS. Humes, 1995. Two source approach for estimating soil and vegetation energy fluxes in observations of directional radiometric surface temperature. Agricultural and Forest Meteorology, 77(3-4): 263-293.
12. Boulet, G., B. Mougenot, J.P. Lhomme, P. Fanise, Z. Lili-Chabaane, A. Olioso, M. Bahir, V. Rivalland, L. Jarlan, O. Merlin, B. Coudert, S. Er-Raki and J.P. Lagouarde, 2015. The SPARSE model for the prediction of water stress and evapotranspiration components from thermal infra-red data and its evaluation over irrigated and rainfed wheat. Hydrol Earth Syst Sci Discuss., 12: C3855-C3867.
13. Choi, M., W.P. Kustas, M.C. Anderson, R.G. Allen, F. Li and J.H. Kjaersgaard, 2009. An intercomparison of three remote sensing-based surface energy balance algorithms over a corn and soybean production region (Iowa, U.S.) during SMACEX. Agricultural and Forest Meteorology, 149: 2082-2097.
14. Hamimed, A., L. Nehal, A. Khaldi and H. Azzaz, 2014. Contribution à la spatialisation de l'évapotranspiration d'un agro-système semi-aride en Algérie par utilisation de la télédétection et du modèle METRIC. Physio-Géo. Géographie physique et Environnement, 8: 197-213.
15. Bekkoussa, B., M. Meddi and H. Jourde, 2008. Forçage climatique et anthropique sur la ressource en eau souterraine d'une région semi-aride : cas de la plaine de Mascara, nord-ouest algérien. Revue. Sécheresse, 19(3): 173-184.
16. Hamimed, A., 2009. Suivi de l'état hydrique d'une région semi-aride dans l'ouest algérien à partir des images de télédétection haute et faible résolution. Ph.D. Thesis, Tlemcen University, Algeria, pp: 179.

17. Kustas, W., B. Choudhury, M.M.R. Reginato, R. Jackson, L. Gay and H. Weaver, 1989. Determination of sensible heat flux over sparse canopy using thermal infrared data. Agricultural and Forest Meteorology, 44: 197-216.
18. Qualls, R.J. and W. Brutsaert, 1996. Effect of vegetation density on the parameterization of scalar roughness to estimate spatially distributed sensible heat fluxes. Water Resources Research, pp: 32.
19. Moran, M.S., T.R. Clarke, Y. Inoue and A. Vidal, 1994. Estimating crop water deficit using the relation between surface-air temperature and spectral vegetation index. Remote Sensing of Environment, 49(3): 246-263.
20. Allen, R.G., L.A. Pereira, D. Raes and M. Smith, 1998. Crop evapotranspiration guidelines for computing crop water requirements. FAO Irrigation and Drainage Paper, no. 56. FAO, Rome, Italy, pp: 300.
21. Carlson, T.N., R.R. Gillies and T.J. Schmugge, 1995. An interpretation of methodologies for indirect measurement of soil water content. Agricultural and Forest Meteorology, 77: 191-205.
22. Jiang, L. and S. Islam, 2001. Estimation of surface evaporation map over southern Great Plains using remote sensing data. Water Resources Research, 37: 329-340.
23. Sandholt, I., K. Rasmussen and J. Andersen, 2002. A simple interpretation of the surface temperature/vegetation index space for assessment of surface moisture status. Remote Sensing of Environment, 79(2): 213-224.
24. Priestley, C.H.B. and R.J. Taylor, 1972. On the assessment of surface heat flux and evaporation using large-scale parameters. Monthly Weather Review, 100: 81-92.
25. Flint, A.L. and S.W. Childs, 1991. Use of the Priestley-Taylor evaporation equation for soil water limited conditions in a small forest clearcut. Agricultural and Forest Meteorology, 56(3): 247-260.
26. Boegh, E., H. Soegaard and A. Thomsen, 200.) Evaluating evapotranspiration rates and surface conditions using Landsat TM to estimate atmospheric resistance and surface resistance. Remote Sensing of Environment, 79(2): 329-343.
27. Seguin, B., S. Baelz, J.M. Monget and V. Petit, 1982. Utilisation de la thermographie IR pour l'estimation de l'évapotranspiration régionale. I.- mise au point méthodologique sur le site de la Crau. Agronomie, 2: 7-16
28. Kustas, W.P. and J.M. Norman, 1999. Evaluation of soil and vegetation heat flux predictions using a simple two-source model with radiometric temperatures for partial canopy cover. Agricultural and Forest Meteorology, 94(1): 13-29.
29. Teixeira, A.D.C., W.G.M. Bastiaanssen, M. Ahmad and M.G. Bos, 2009. Reviewing SEBAL input parameters for assessing evapotranspiration and water productivity for the Low-Middle Sao Francisco River basin, Brazil: Part A: Calibration and validation. Agricultural and Forest Meteorology, 149(3): 462-476.
30. Choi, M., T.W. Kim, M. Park and S.J. Kim, 2011. Evapotranspiration estimation using the Landsat-5 Thematic Mapper image over the Gyungan watershed in Korea. International Journal of Remote Sensing, 32(15): 4327-4341.
31. Bastiaanssen, W.G.M., T. Van Der Wall and T.N.M. Visser, 1996. Diagnosis of regional evaporation by remote sensing to support irrigation performance assessment. Irrigation and Drainage Systems, 10: 1-23.
32. Bougeault, P., J. Noilhan, P. Lacarrere and P. Mascart, 1991. An experiment with an advanced surface parameterization in a mesobeta-scale model. Part I: Implementation. Monthly Weather Review, 119(10): 2358-2373.